substance: Nb_2O_5
property: defect and transport properties

The departure of H–Nb_2O_{5-x} from stoichiometry as a function of temperature and pressure has been extensively studied [61K, 68K, 65B, 72N, 69S, 68A, 73K, 74M, 76K, 79M]. The earlier results at lower temperatures suggested that the defect concentrations varies as $p_{O_2}^{-1/4}$ near stoichiometry and at $p_{O_2}^{-1/6}$ at lower oxygen pressures. This can easily be explained with a point defect model as: $O_0 \leftrightarrow V_0 + 1/2\ O_2$ (H_v), $V_0 \leftrightarrow V_0^{\cdot} + e^-$ (ε_1), $V_0^{\cdot} \leftrightarrow V_0^{\cdot\cdot} + e^-$ (ε_2). If the dominant defects are $V_0^{\cdot}$ we expect $[V_0^{\cdot}] \propto p_{O_2}^{-1/4}$ and if the dominant defects are $V_0^{\cdot\cdot}$ we expect a $p_{O_2}^{-1/6}$-law. Analysis of the temperature variation of the stoichiometry from thermal measurements gives

$H_v + \varepsilon_1 + \varepsilon_2$	105.8 kcal mol^{-1}	74M
	103 kcal mol^{-1}	62K

At 1100ºC, a discontinuity in resistance was found [79M] corresponding to the formation of a new phase (see below).

This simple view of point defects extending over a substantial stoichiometric range has been strongly challenged [72N, 73K]. Typical stoichiometry data are shown in Figs. 1 and 2 and at very high temperature a series of breaks in the curve [73K] strongly support the idea that a significant number of quite distinct phases can form. Combined structural and thermal experiments at 1000ºC [72N] reveal the following domains for NbO_x:

(1) $2.500 \geq x \geq 2.495$. Only the single phase H-Nb_2O_{5-x} found without any local rearrangement or extended Wadsley defects. It is probable that in this range point defect theory may be used.
(2) $2.495 > x \geq 2.480$. Two phases found corresponding to H-Nb_2O_5 and $Nb_{25}O_{62}$.
(3) $2.480 > x \geq 2.417$. Two phases found corresponding to $Nb_{25}O_{62}$ and $Nb_{12}O_{29}$ (monoclinic).

Thus, at 1000ºC, the reduction traverses the route H-$Nb_{28}O_{70} \rightarrow Nb_{25}O_{62} \rightarrow Nb_{12}O_{29}$. The structural relationship between these three phases is shown in Fig. 3. Thus, although Fig. 1 apparently shows typical bivariant behaviour for the 900ºC and 1000ºC results, the material present for $x \leq 2.495$ is inhomogeneous; only at $x = 2.480$ did there appear to be a single phase: the $Nb_{25}O_{62}$ structure. The apparently bivariant behaviour must thus be traced to extremely slow kinetics [72N].

At higher temperatures, a quite different type of behaviour is observed. In addition to the definite phases $Nb_{28}O_{70}$ (i.e. H-Nb_2O_5) and $Nb_{25}O_{62}$, a phase formed as an intergrowth, $Nb_{53}O_{132}$ can form. The process of intergrowth is shown schematically in Fig. 4, which shows the regular intergrowth phase $Nb_{53}O_{132}$ as a natural intermediate. The important point about these intergrowth phases is that, unlike the nucleation (presumably at isolated Wadsley defects) and subsequent growth of $Nb_{25}O_{62}$ from H-Nb_2O_5, considerable activation energy is needed to form the (thermodynamically more stable) $Nb_{53}O_{132}$. A similar intergrowth, $Nb_{47}O_{116}$, forms between $Nb_{25}O_{62}$ and $Nb_{12}O_{29}$ (Fig. 4). The reduction sequence at high temperatures is then $Nb_{28}O_{70} \rightarrow Nb_{53}O_{132} \rightarrow Nb_{25}O_{62} \rightarrow Nb_{47}O_{116} \rightarrow Nb_{23}O_{54} \rightarrow Nb_{12}O_{29}$. A considerable trivariant regime therefore still remains at high temperature, and materials formulated as $Nb_{22}O_{54-x}$ and $Nb_{25}O_{62-x}$ show quite wide ranges for x (Figs. 5, 6) as well as $Nb_{28}Sb_{70-x}$ itself. It can be seen that in the bivariant region $[V_0]_{tot} \propto p_{O_2}^{-1/2}$, where $[V_0]_{tot} = x/54$ for $Nb_{22}O_{54-x}$ and $x/62$ for $Nb_{25}O_{62-x}$.

The nature of the point defects in Nb_2O_{5-x} has been controversial even over the area where a single definite phase is seen and $[V_0]tot \propto p_{O_2}^{-1/4}$. In addition to singly charged oxygen vacancies, interstitial Nb ions have been proposed in both N-Nb_2O_5 [72H] and H-Nb_2O_5 [73A]. For the latter, the interstitial tetrahedral Nb represents an attractive structural option; thermodynamically $Nb_{Nb} + 5/2\ O_O \leftrightarrow Nb_i^{n\cdot} + ne^- + 5/2\ O_2$. Hence, for Nb_2O_{5-x}, $x \propto p_{O_2}^{-5/4(n+1)}$ and the observed $p_{O_2}^{-1/4}$ dependence can be accounted for with n = 4. However, the change to a slope of – 1/6 cannot be explained on a point defect interstitial Nb model.

In the $p_{O_2}^{-1/4}$ region, the activation energy for deviation from stoichiometry is found to be 3.10 eV in ceramic samples of H-Nb_2O_5 [73B] whereas the resistance varies as in Fig. 7 with an activation energy of 1.65 eV [62K, 73B]. This suggests a slightly activated mobility, $E_A(\mu) \approx 0.10$ eV and $\mu(1100^oC) \approx 0.10$ cm^2/V s [73B]. The Seebeck coefficient also suggests a low activation energy [73B].

In the $p_{O_2}^{-1/6}$ region, the thermogravimetric studies show an activation energy of 4.46 eV, for the formation of doubly ionized oxygen vacancies in H–Nb_2O_5 [62K]. The actual conductivity in this region shows a lower apparent activation energy (Fig. 8), which can be satisfactorily explained by allowing the mobility $\mu \propto T^{-3}$ (Fig. 9), a result consistent with normal optical-mode scattering [59S].

There are a number of puzzling features about the interpretation in terms of singly-ionized oxygen vacancies [62K], and we would tentatively suggest that the transition from the $p_{O_2}^{-1/4}$ to $p_{O_2}^{-1/6}$ regions may correspond to a transition from interstitial $Nb_i^{4\cdot}$ to doubly ionized oxygen vacancies ($V_0^{\cdot\cdot}$).

At higher temperatures, the conductivity shows marked discontinuities (Fig. 10) corresponding to the formation of new phases. The resistivity continues to show a $p_{O_2}^{-1/6}$ behaviour in this region, suggesting the presence of doubly ionized oxygen vacancies [74M].

References:

59S Scanlon, W. W.: Solid State Phys. 9 (1959) 83.
61K Kofstad, P., Anderson, P. B.: J. Phys. Chem. Solids 21 (1961) 280.
62K Kofstad, P.: J. Phys. Chem. Solids 23 (1962) 1571.
65B Blumenthal, R. N., Moser, J. B., Whitmore, D. H.: J. Am. Ceram. Soc. 48 (1965) 617.
68A Abbatista, F., Chientaretto, G., Tkachenko, E. V.: Atti Accad. Sci. Torino Cl. Sci. Fis. Mat. Nat. 102 (1968) 866.
68K Kofstad, P.: J. Less-Comm. Met. 14 (1968) 153.
69S Schäfer, H., Bergner, D., Gruehn, R.: Z. Anorg. Allgem. Chem. 365 (1969) 31.
72H Hutchinson, J. L., Anderson, J. S.: Phys. Status Solidi (a) 9 (1972) 207.
72N Nimmo, K. M., Anderson, J. S.: J. Chem. Soc. Dalton Trans. 1972, 2328,
73A Anderson, J. S., Browne, J. M., Cheetham, A. K., von Dreele, R., Hutchinson, J. L., Lincoln, F. J., Bevan, D. J. M., Straehle, J.: Nature 243 (1973) 81.
73B Le Brusq, H., Delmaire, J. P.: Rev. Int. Hautes Temp. Refract. 10 (1973) 15.
73K Kimura, S.: J. Solid State Chem. 6 (1973) 438.
74M Marucco, J. F.: J. Solid State Chem. 10 (1974) 211.
76K Kikuchi, T., Goto, M.: J. Solid State Chem. 16 (1976) 363.
79M Marucco, J. F.: J. Chem. Phys. 70 (1979) 649.

Fig. 1.

NbO. Composition parameter x vs. oxygen pressure. Solid lines: [72N]; full and open circles: [65B]; dashed lines: [61K]; triangles: [68A]; 1300°C isotherm [69S]. Fig. from [72N]. 1 atm ≈ 1 bar.

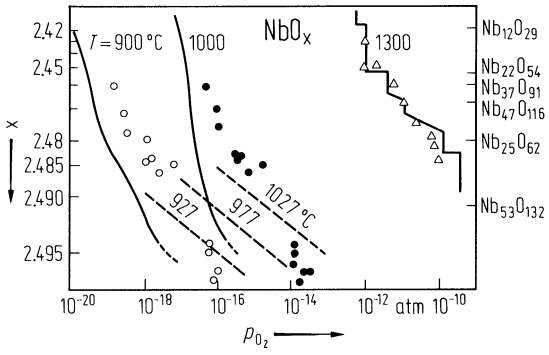

Fig. 2.

NbO_x. Oxygen partial pressure vs. composition at 1300ºC and 1400ºC [76K].

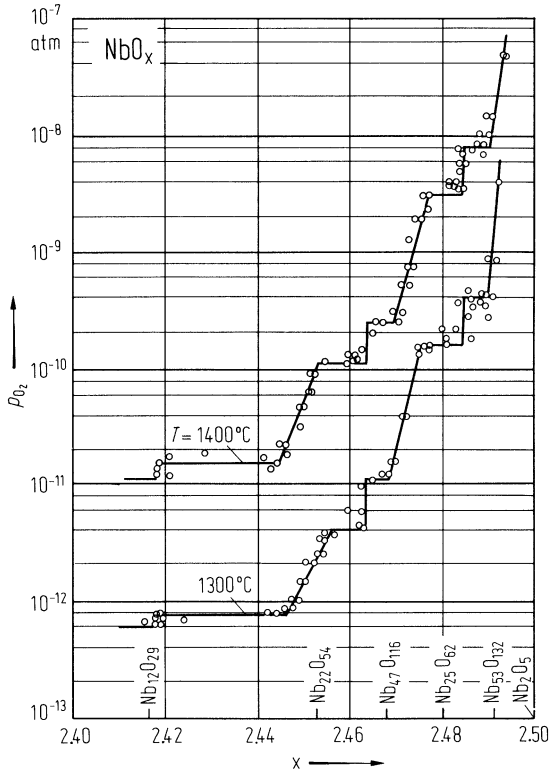

Fig. 3.

Structural relationship between (a) $Nb_{12}O_{29}$, (b) $Nb_{25}O_{62}$ and (c) H-Nb_2O_5 in (010) projection [72N].

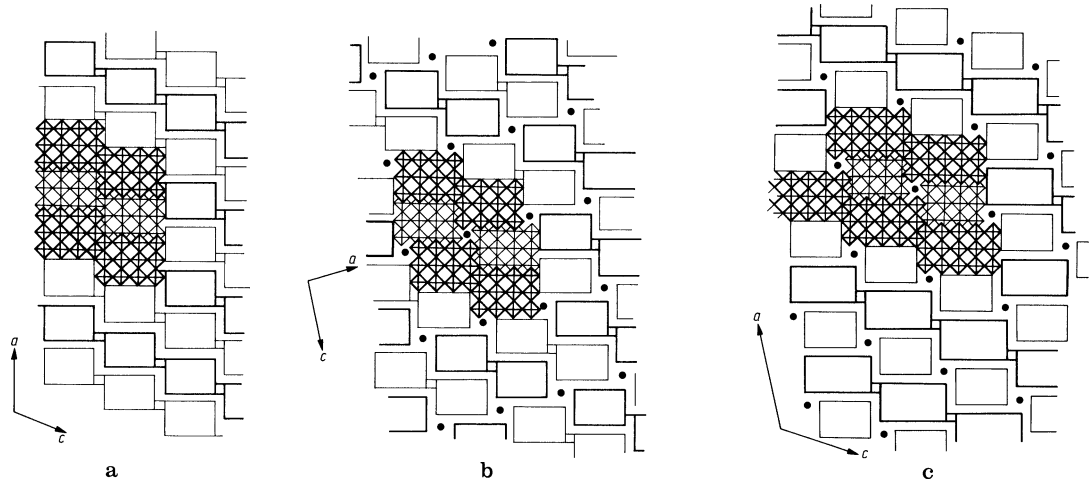

Fig. 4.

Mechanisms whereby intergrowth phases may form at high temperatures. (a) coherent intergrowth of one row of $Nb_{25}O_{62}$ in H-Nb_2O_5; (b) coherent intergrowth of one row of $Nb_{12}O_{29}$ in $Nb_{25}O_{62}$; (c) regular coherent intergrowth corresponding to the phase $Nb_{53}O_{132}$ [72N].

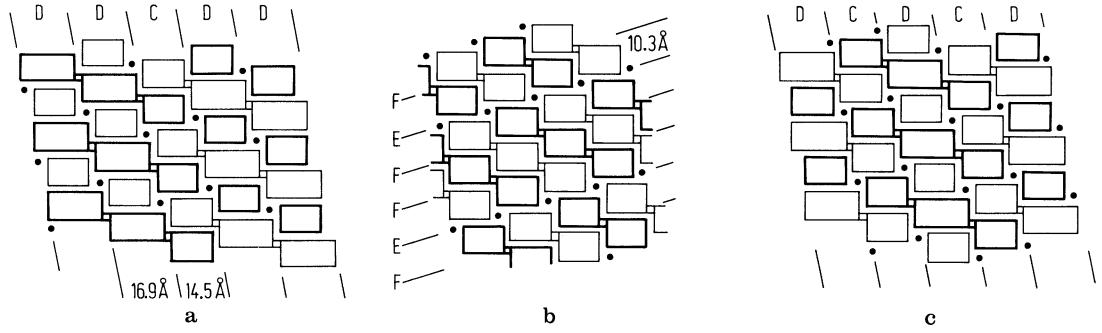

Fig. 5.

$Nb_{22}O_{54-x}$. Total vacancy concentration vs. oxygen pressure. $[V_O]_{tot}$ = x/54 [76K]. Open triangles are data derived from Nb_2O_5 and dots are those derived from NbO_2.

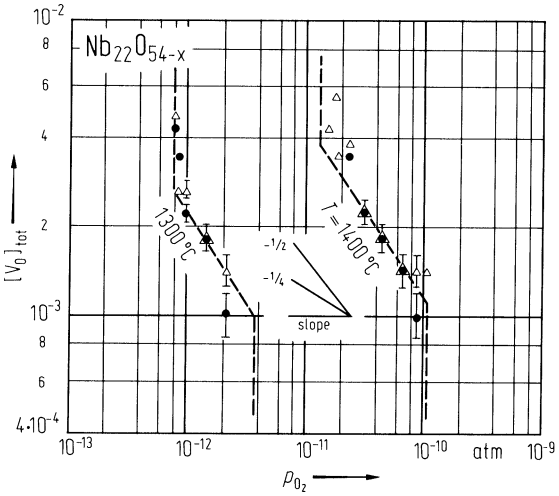

Fig. 6.

$Nb_{25}O_{62-x}$. Total vacancy concentration vs. oxygen pressure. $[V_O]_{tot}$ = x/62 [76K]. For triangles and dots , see caption of Fig. 5.

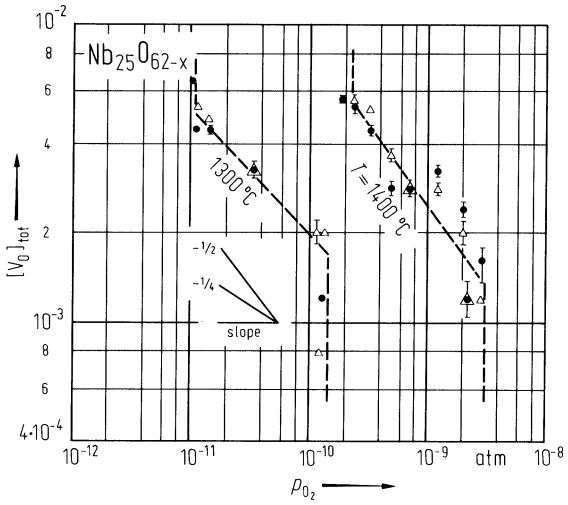

Fig. 7.

α-Nb_2O_5. Resistance vs. (reciprocal) temperature at 1 atm ($p_{O_2}^{-1/4}$ region) [62K].

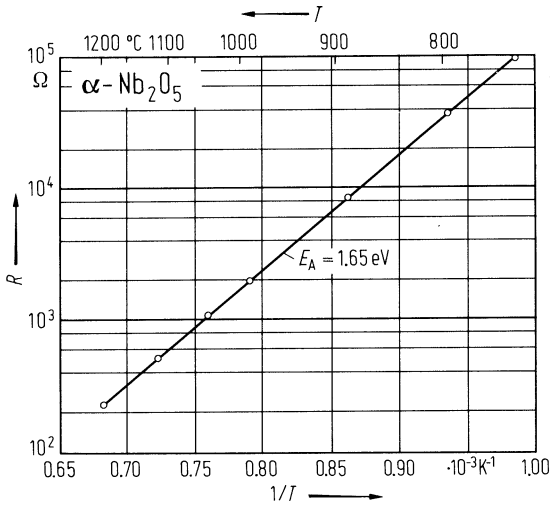

Fig. 8.

α-Nb_2O_5. Resistance vs. (reciprocal) temperature at $p_{O_2} = 10^{-13}$ atm ($p_{O_2}{}^{-1/6}$ region) [62K].

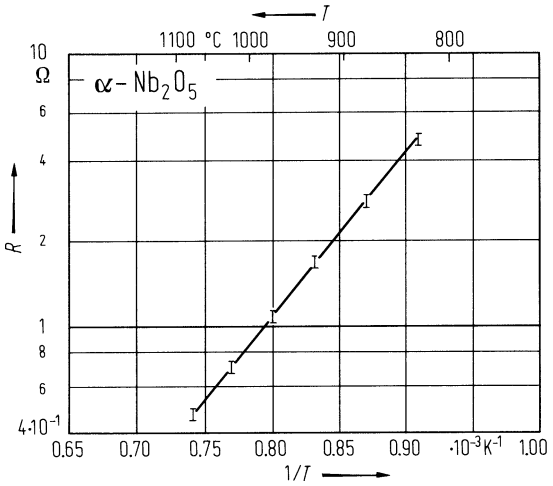

Fig. 9.

α-Nb_2O_5. Electron drift mobility vs. temperature for ceramic sample at p_{O_2} = 10^{-13} atm showing $\mu \propto T^{-3}$ [62K].

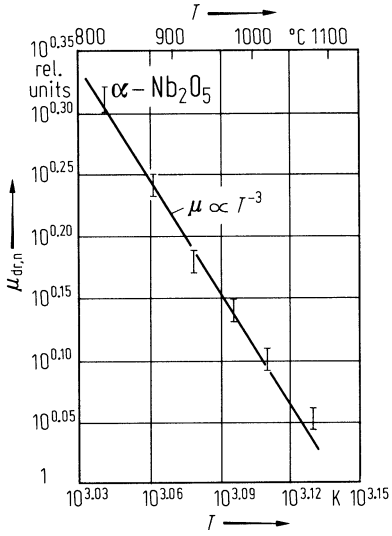

Fig. 10.

α-Nb_2O_5. Resistance vs. oxygen pressure at 100ºC. Full circles: Nb_2O_{5-x} (stable phase); open circles: metastable phase of Nb_2O_{5-x}, open triangles: stable phase of $Nb_{25}O_{62-x}$, full triangles: $Nb_{12}O_{29-x}$, squares: metastable phase of oxidation of $Nb_{12}O_{29-x}$ [74M].